Tectonic Critical Phenomena with Dilatancy in Analogue Models

Gerd Gudehus [1)] and Christof Lempp [2)]

1) Institute of Soil and Rock Mechanics, Karlsruhe Institute of Technology, Gerd.Gudehus@kit.edu
2) Institute of Geosciences and Geography, Martin Luther University Halle-Wittenberg, christof.lempp@geo.uni-halle.de

Keywords: saddle and tipping points, tectonic dislocations, fractality and fractionality, shear bands and cracks, stress-dilatancy, mechanical chain reactions, analogue models

Abstract

The dilatancy of soil and rock eludes continuum mechanics, thermodynamics and materials science as it is localized in fractal patterns of shear bands (faults) and/or cracks. As far as shear bands dominate it is captured by a driven succession of saddle points of the specific elastic energy, which are equivalent to a Mohr-Coulomb condition with effective stress, growing friction and waning cohesion. A driven dilatation turns into a spontaneous contraction when the energy reaches a tipping point with regard to the pore volume, then the pore water pressure grows and the stress deviator drops. The implied state variables and rates are defined as quasi-local and -momentary by means of fractional derivatives. Energy-based constitutive equations include a relation of stress and dilatancy with maximal dissipation, while rockburst with dominant cracks is excluded by a criterion. Successions of driven dilatation and spontaneous contraction imply seismogenic mechanical chain reactions, which are enhanced by seismic waves and spreading of pore water. Such mechanisms are observed in sandbox and cell tests, which serve as analogue models beyond usual similarity rules. The scale-independence of features thus obtained is validated in the companion paper on lithosphere sections.

1 Introduction

The ancient Greek word $\kappa\rho\iota\sigma\iota\varsigma$ (crisis) means moment of decision. More specifically in a physical sense, it means a bifurcation at an energetically defined critical point. For instance, the gravitational energy of a sphere upon an open hand is at tipping points along the rim and at a saddle point upon the wrist; in both cases it rolls inwards or outwards. If water in a box is at a critical point the transition energy from liquid to vapor vanishes, then bifurcations from thermodynamic equilibria lead to bubbles and drops with a fractal size distribution. *Tectonic critical phenomena* in the lithosphere are

more intricate as this system is not conservative: differently to molecules, rock fractions and their arrangement change with a loss of potential energy. $\tau\epsilon\kappa\tau\omega\nu$ (tecton) means builder and mover, in this sense tectonic evolutions may be understood as structure-forming and -erasing critical phenomena. The pore system of rock with faults and cracks is permeable: $\pi o\rho o\varsigma$ (poros) means passage, this is extremely variable. Thus effective pressures decrease by a growing pore pressure if the total pressure does not change. Rock has fractal features due to former critical phenomena, so how to explain changes of solid state and pore system with the aid of successive critical points?

Reynolds (1885) coined the notion *dilatancy* for the dilatation of dense grain fabrics by shearing with constant overall pressure. Taylor (1948) observed that the ratio of shear stress and effective pressure by shearing grows with dilatancy. Referring to triaxial tests with sand, Rowe (1962) showed that the ratio of principal stress components is inversely proportional to the ratio of inelastic strain rate components. Leaving aside that the dilatancy is always localized in shear band patterns (Desrues et al. 2007) and that it comes in jerks, such stress-dilatancy relations work with spatially averaged stress and strain rate components after smoothing-out fluctuating experimental plots. With reverse shearing the ratio of shear stress and effective pressure drops, and the dilatancy gets negative by turning into *contractancy*. Thus shear bands can be erased, and the pressure of pore water grows by a rapid contraction so that a water-saturated grain fabric can turn into a mush.

Kadanoff (1966) proposed a 'renormalization group' method for thermodynamic critical phenomena which exhibit *fractality*. Later he tried to apply his method to granular flow, but concluded that this does not work and that integral equations are required (Kadanoff 1999). Leaving aside fractal features, Jiang and Liu (2009) proposed a constitutive model by means of an additional granular temperature and a conjugated granular entropy. Thus dilatancy is obtained beyond a saddle point of the elastic energy with regard to invariants of elastic strain, which is equivalent to a Mohr-Coulomb condition. Replacing the granular temperature by a sensitivity of the grain fabric and modifying the elastic energy, Gudehus (2019) captured dilatancy and contractancy up to a decay with pore water or during a densification in shear cycles. Shear localization and jerks are again left aside by spatial averaging and smoothing out. Boxes with sand, clay or similar matter are often used as *analogue models* of tectonic evolutions. Following Hubbert (1937), rules of mechanical similarity are applied, inferring constitutive relations of soil mechanics or rheology. Interpreting shear bands as faults, patterns of the former resemble those in the lithosphere, and combining their orientations with a Mohr-Coulomb condition stress fields can be estimated (Mandl 1988). However, such stresses are *not the ones proposed by* Cauchy (1827) as his volume elements are not compatible with shear bands. Model tests with cohesive powder can produce also crack patterns which resemble those observed in situ (Holland et al. 2006), but this kind of fractally

localized dilatancy eludes likewise present mathematical methods. So how could fractal patterns of shear bands and cracks, which arise in model tests like in the lithopshere, be explained by means of critical phenomena?

Pointing to fractal distributions from logging along boreholes, Leary (1997) concluded that the lithosphere is in a subcritical state. He argues that rock is no 'engineered' (i.e. technically processed) material because of divergent correlation lengths, i.e. as fluctuation wavelengths diverge. In other words, *rock is no simple material* in the sense of Truesdell and Noll (2004) as constitutive relations are not locally confined. Spatial and temporal distributions with fractal fluctuations cannot be smoothed out so that they are *not differentiable*, and - as outlined by Jiang and Liu (2009) - *thermodynamic potentials do not suffice*. Therefore tectonic critical phenomena with dilatancy cannot be sufficiently captured with materials science, thermodynamics and continuum mechanics. Especially, the representation of rock joints by shear bands in numerically simulated grain fabrics with cohesion by Ord and Hobbs (2010), and their use of thermodynamics and instabilities with differential equations for getting fractal patterns, are questionable.

Alejandro and Alonso (2005) tried to capture the relation of dilatancy and stress for rock by means of elasto-plastic models. Speaking of loading, strength, damage and failure, Cieslik (2018) proposed a similar approach. However, rock is rather clastic than plastic, and not a simple (or technically processed) material. The lithosphere is not loaded nor damaged and cannot fail like a technical structure, and strength is an inadequate notion. Moreover, dilatation and contraction of the pore system require a redistribution of pore water, which is related with tectonic stressing or relaxation. So which features observed with analogue models, including rock samples and pore water, can capture critical phenomena with dilatancy and contractancy and can be scaled up to the lithosphere? And how to define and interpret mean values and coefficients of variation in the light of the wild randomness, visible by divergent fluctuation wavelenghts which characterizes fractality (Mandelbrot 1999) and eludes standard method of statistics?

For comparison we consider first models without dilatancy (Sect. 2). Then we turn to sand, clay and similar matter in experimental setups which can serve as tectonic analogue models (Sect. 3). Thereafter uniaxial, triaxial and biaxial tests with samples of sandstone and granite are likewise evaluated as analogue models (Sect. 4). In both sections fractal features are first left aside by means of overall quantities, then taken into account by means of quasi-local and -momentary quantities defined with the aid of fractional derivatives. Mathematical details are outlined in an appendix, such a clarification is indispensable despite or just due to the complexity and opacity of geo-matter. The paper ends with conclusions and an outlook (Sect. 5). The scale-independence of the proposed features is outlined in the companion paper on lithosphere sections (Gudehus and Lempp 2022b).

2 Models without dilatancy

Dominoes standing on a table are conserved, but not their energy and arrangement if the latter enables a *mechanical chain reaction*. If the gravitational energy of a tilted domino attains a tipping point it turns over a suitably placed neighbor, and so on until a neighbor stands cross, too close or far off. The successive collapse reduces the void volume between the dominoes, while a part of the potential energy is dissipated into noise and heat. We will see in Sect. 4 that mechanical chain reactions in rock samples are likewise contractant and enhanced by shock waves, and also by pore water, but after stressing with dilatancy, and that they cannot be calculated as with dominoes.

Water at equilibrium in a closed box has a sum of intermolecular potential and thermal kinetic energies which can be represented as a function of pressure p and absolute temperature T. At its critical point ($T_c = 647$ Kelvin and $p_c = 21,7$ MPa) the transition energy from liquid to vapor disappears, therefore drops and bubbles attain sizes with a fractal distribution. During this *critical phenomenon* the molecules and their overall energy are conserved, while their fluctuating velocities turn from a normal (Maxwell-Boltzmann) to a power-law (fractal) distribution. The randomness turns form mild to wild (Mandelbrot 1999) so that fluctuation wavelengths diverge, whereas the latter are confined to a few molecule diameters in the non-critical range. Such thermodynamic critical phenomena with fractality are captured by a renormalization (Kadanoff 1966). However, a one-to-one transfer of this method to the lithosphere (as proposed e.g. by Leary 1997) is not justified as rock fractions and their energies are not conserved.

Critical phenomena of solids (e.g. the change of magnetism at the Ising point) do not leave back traces if crystallites and their arrangement are conserved, but this is no more the case with *dislocations*. Persson (2000a) captures the dependence of stress on strain rate of a pore-free solid with thermally activated dislocations (Appendix A1). A straightforward transfer of his theory to minerals is not feasible as adequate tests with pore-free mineral are not available. However, estimates can be obtained by means of triaxial tests with quartz sand and kaolin clay, wherein strain rates are imposed with amounts changing by at least two orders of magnitude (Gudehus 2011). This leads to a ratio $E_a/k_BT \approx 40$ of activation and thermal energies for quartz and about 15 for kaolin with $T = 293$ K. These are crude estimates as sizes of dislocated crystallite blocks and kinematic relations of soil fabric and mineral strain rates have to be guessed. Persson's (2000a) relations cannot capture tectonic dislocations with divergent fluctuation wavelengths, so we will employ his strain-rate dependence and his lower and upper bounds with reservation.

Sliding of a solid block past a rigid plane implies dislocation and wear so that such a system is not conservative. Persson (2000b) derives Coulomb's friction law by means of minute solid bridges with a total surface proportional to the normal force. A bridge slides off if it reaches a critical point of the sum of elastic and surface energies. This

occurs in a random succession, but so that the total sliding resistance is proportional to the normal force independently of the spatio-temporal distribution of solid bridges.

Persson (2000b) obtains a successive stick-slip, i.e. a kind of *seismicity*, with solid blocks connected by springs when they slide past an idealized fault plane. This theory differs from the Burridge-Knopoff (1967) model, which leads to a kind of Gutenberg-Richter frequency distribution by means of a reduction from halting to sliding friction, but the latter is not energy-based as proposed by Persson. Turcotte (2001) shows that the Burridge-Knopoff model is algebraically equivalent to the theory of Bak et al. (1987) with a 'self-organized criticality'. Such algorithms can yield Gutenberg-Richter-like frequency distributions, but cannot capture tectonic critical phenomena as the algorithms do not imply realistically defined critical points.

The analogies of this section are remote as they do not take into account dilatancy with divergent fluctuation wavelengths. This holds also true for the similarity of electromagnetic and seismic jerks (Dahmen and Ben-Zion 2009). Nevertheless dominoes on a table constitute a prototype of mechanical chain reactions, thermally activated dislocations delimit the rate-independence of tectonic critical phenomena, and plane arrays of slider blocks with springs can yield Gutenberg-Richter-like frequency plots although such models cannot properly represent the lithosphere.

3 Analogue models with granular matter

An early sandbox test

George Darwin (1883) - second son of Charles Darwin, astronomer and mathematician - carried out experiments with dry flint flour in a box. He filled it up to different heights and released a string with a spring-balance which kept a movable wall with a hinge, and observed a decrease of the string force during the release up to a breakdown of equilibrium. The latter - called 'capricious' as it could not be repeated quantitatively - was indicated by a sudden rise of the string force and a hissing noise. Darwin's findings refuted theories of his time with limit stress fields, whereas his limit earth pressures matched those by Coulomb's (1776) theory. He got the advice from Clerk Maxwell that 'a *historical element* would enter largely into the nature of the limiting equilibrium of sand', and concluded that this would 'essentially elude mathematical treatment'.

Darwin (1883) observed a *driven dilatation* (called unsettling) up to a *spontaneous contraction* (settling) of the grain fabric under nearly constant pressure, so - except wording - he discovered dilatancy before Reynolds (1885), and also contractancy. His findings were largely ignored, and until present there are no calculation models which could reproduce them. His experiments exhibit features which are similarly observed in

the lithosphere: the horizontal stretching of the grain fabric due to the yielding of a wall resembles a tectonic extension, and the hissing noise during the thus attained collapse indicates micro-seismic P-waves with a frequency $f \approx 10^3$ s^{-1} and more, i.e. wavelengths up to $c_p/f \approx 10^{-1}$ m nearly like the layer thickness of flint powder with $c_p \approx 100$ ms^{-1}.

Limit states and shear bands of sand

Casagrande (1936) proposed stationary 'critical states' of dry sand sheared in a box with the Coulomb limit condition (a misnomer as Coulomb did not know Cauchy's stress)

$$\tau = \sigma \tan \phi_r \tag{1}$$

for shear stress τ and normal stress σ with a residual friction angle ϕ_r and a critical void ratio $e_c(\sigma)$. Roscoe (1970) observed *dilatated shear bands* with about 10 grains thickness and non-uniform stress distributions in sheared sand samples, concluding that uniform and stationary 'critical states' are not attainable. Biaxial tests with fixed smooth confining plates yield a shear band which is visible by offsets of the confining membrane (Gudehus 2011). Its inclination against the major principal stress σ_1 is $\theta \approx 45^0 - \phi/2$ as by (1) and the tangent to a stress circle. Analyses of a quasi-static bifurcation from uniform deformation to localized dilated shearing yield similar θ-values (Kolymbas 1981, Vardoulakis 1996).

X-ray tomographies reveal *fractal shear band patterns* which evolve alongside with dilatancy in biaxial tests so that eventually one shear band dominates (Desrues et al. 2007). Such bands are reproduced numerically with about ten grains thickness by means of inter-granular rotations and an initial fluctuation of the void ratio (Nübel 2002). Moreover, if a membrane on a rigid base under a layer of originally dense sand is extended a pattern of crossing shear bands is obtained with $\theta \approx \pm(45^0 - \phi/2)$ against the vertical stress and a distance of about 1/4 of the layer thickness, while the surface exhibits grabens and rifts. With a further extension secondary smaller shear bands arise, while tertiary ones are not achieved as a quasi-static continuation gets impossible, which indicates an impending collapse. Such a *fractal uniformity* is not achieved in general: for instance, shear band patterns observed with X-rays during triaxial tests wane towards the sample axis and the endplates (Desrues et al. 2007).

Shear bands arise likewise in *water-saturated* sand, for which Terzaghi's (1936) relation

$$\sigma = \sigma' + p_w \tag{2}$$

of total stress σ, effective stress σ' and pore water pressure p_w determines the interaction of grain fabric and pore water. (2) results from the neutrality of the grain mineral with respect to changes of p_w (GUDEHUS 2020). Dilatating shear bands take up pore water so that its pressure p_w is reduced, but this reduction is minor with drainage as long as the time of overall deformation exceeds the time needed for regaining a hydrostatic p_w. A contractant collapse after an overall dilatation up to a tipping point causes a sudden rise of p_w, this can lead to a decay of the grain fabric, i.e. to $\sigma' \to 0$ via (2) by $p_w \to \sigma$.

Energy-based constitutive relations for sand

JIANG AND LIU (2009) propose an *elastic energy* w_e per unit of grain fabric volume (or specific) as a function of elastic strain ϵ^e_{ij} and void ratio e. w_e is the potential of the effective stress by

$$\sigma'_{ij} = (1-\mu)\frac{\partial w_e}{\partial \epsilon^e_{ij}}, \tag{3}$$

wherein μ increases with a granular temperature T_g from zero for rest to $\mu_h \approx 0.8$ for a hypoplastic range (hypo=sub). w_e has saddle points with regard to invariants of ϵ^e_{ij} which are equivalent to a Mohr-Coulomb condition without cohesion. $d\epsilon^e_{ij}$ grows with the total strain increment $d\epsilon_{ij}$ by the same reduction factor $1-\mu$, and decreases in proportion to $d\epsilon \equiv |d\epsilon_{ij}|$, ϵ^e_{ij} and T_g. These relations are derived with Onsagers' symmetry for the thermal entropy production, therein a specific granular entropy $s_g \propto T_g^2$ is proposed for enabling stable equilibria.

In a modification of this theory (GUDEHUS 2019) w_e has similar saddle points, but the equation for $d\epsilon^e_{ij}$ is adapted to the actual rate-independence (i.e. $d\epsilon^e_{ij}(\lambda d\epsilon_{ij}) = \lambda d\epsilon^e_{ij}(d\epsilon_{ij})$ for $\lambda > 0$). T_g is replaced by the intensity χ of spatial fluctuations of the elastic energy, which is equivalent to the sensitivity or *eutaraxy* χ ($\epsilon\upsilon$=favoring, $\tau\alpha\rho\alpha\xi\iota\varsigma$=disturbance). χ grows with a monotonous deformation from at least 0 to a maximum χ_h in the hypoplastic range, while μ grows via $\mu = \mu_h\chi/\chi_h$. χ and μ dwindle with a reversal of strain path, more so with many reversals of small amplitude, and rise again with monotonous deformations.

(3) is taken over by GUDEHUS (2019), which means that a major part of the elastic energy is quenched in spatial fluctuations - like with glassy matter (SORNETTE 2000) - so that it does not contribute to the force-transferring effective stress. This disordered energy is proportional to a specific *configuration entropy* $s_\chi \propto \chi^2$ instead of s_g by JIANG AND LIU (2009). A reduction factor $1-\mu$ both for average force and relative velocity is similarly achieved in a bicycle by a transmission belt with stick-slip upon smooth wheels instead

of a chain upon indented wheels. The specific elastic energy w_e can reach a tipping point with regard to the void ratio e, then a dry grain fabric collapses with contraction and a water-saturated one turns into a mush.

As outlined in Appendix A3, this approach works also with fractally uniform shear band patterns, then the state variables $\hat{\epsilon}^e_{ij}$ (or equivalently $\hat{\sigma}'_{ij}$), $\hat{n}$ (or $\hat{e} = \hat{n}/(1+\hat{n})$) and $\hat{\chi}$ are *quasi-local quantities*. They are mean values for an inspection cube which dwindle with its size by a power-law, except $\hat{\chi}$ which is proportional to the coefficient of variation; both properties characterize the spatial fractality (A2). The elastic energy $\hat{w}_e(\hat{\epsilon}^e_{ij})$ works as potential of the effective stress as by (3). Quasi-local quantities for fractally uniform sections are reconciled with non-fractal spatial trends by means of fractional gradients which vanish with fractal uniformity (A2). This approach requires a reference length, which serves also as lower bound of inspection cube sizes with fractality and provide independence of length units.

A stress-dilatancy relation despite shear bands and jerks

In a Mohr-Coulomb condition with an $\hat{n}$-dependent friction factor $\tan\phi'$ (A3) this exceeds the residual $\tan\phi'_r$ by (1) due to the dilatancy with shear bands. With cylindrical symmetry driven successions of such saddle points of the elastic energy can be captured by the *stress-dilatancy* relation (Rowe 1962)

$$\frac{\hat{\sigma}'_1}{\hat{\sigma}'_3} = -2\tan^2(\pi/4 + \phi'_r/2)\frac{d\hat{\epsilon}^i_3}{d\hat{\epsilon}^i_1}. \tag{4}$$

Therein $d\hat{\epsilon}^i_1$ and $d\hat{\epsilon}^i_3$ denote increments of inelastic axial and radial overall strain $\hat{\epsilon}^i_3$ and $\hat{\epsilon}^i_1$, derived from smoothed-out plots of $\hat{\epsilon}_3$ versus $\hat{\epsilon}_1$. Quasi-local quantities in (4) mean that thickness and pattern of shear bands do not matter for the relation of stress and dilatancy, which is legitimate as overall force and velocity ratios do not depend on spatial fluctuations of inter-granular forces and velocities. With our constitutive model the rate of dissipation is proportional to the eutaraxy $\hat{\chi}$, and maximal with $d\hat{\epsilon}^i_3/d\hat{\epsilon}^i_1$ by (4) for a given $\hat{\sigma}'_1/\hat{\sigma}'_3$ (A3). This behavior can be attributed to successive incremental steepest descents of the elastic energy from saddle points. Dilatancy with stressing, and also contractancy with unstressing, is captured by the same constitutive model not only with axial symmetry.

Using thermography Luong (1982) observed a flash-heating up to ca 1000^0 C at quartz grain contacts. This kind of heating requires an inter-crystalline strain rate $\dot{\epsilon} > 10^{10}$/s (A1), while the overall strain rate was $\dot{\hat{\epsilon}} \approx 10^{-4}$/s, which indicates that dislocations of crystallites can temporarily and locally be up to about 10^{14} times faster than rearrange-

ments of the grain fabric. Together with the crackling or hissing noise these findings show that rearrangements of grain fabrics evolve with jerks.

Tectonic analogue models with sand

The proposed concept enables a scaling up from *micro-tectonic sandbox tests* with similarity rules beyond those proposed by HUBBERT (1937). Inspection cubes with fractal patterns of shear bands (mini-faults) can be employed for defining a quasi-local effective stress tensor $\hat{\sigma}'_{ij}$, which is related with a quasi-local elastic strain tensor $\hat{\epsilon}^e_{ij}$ via an elastic energy (A3). Both tensors are not the ones proposed by CAUCHY (1827) with an infinitesimal volume element as this gets impossible with shear bands. With assumed symmetry both tensors can be represented by principal values, principal directions and Mohr circles. Similarities of fault and shear band patterns (MANDL 1988) speak for a scale-independent Mohr-Coulomb condition with an angle $45^0 - \phi/2$ between $\hat{\sigma}'_1$ and shear bands. Stress-dilatancy relations and coaxiality of stress and stretching rate imply time-stretching invariance and maximal dissipation (A3).

Biaxial tests can serve as analogue models with fractality although their boundary conditions may differ more from those of lithosphere sections than with sandbox tests. Referring to his pioneer investigations of shear banding in sand, VARDOULAKIS (1996) explained the formation of a single shear band as a quasi-static bifurcation by means of an elasto-plastic constitutive relation. VARDOULAKIS AND SULEM (1996) extended this approach to rock, though without fractality. KOLYMBAS (1981) proposed a similar analysis with a hypoplastic constitutive model. Later he questioned the employed principle of local action because of fractality (KOLYMBAS 2003). However, his calculation of shear band inclinations remains valid despite fractal shear band patterns (DESRUES et al. 2007) as the eigenvalue problem of a quasi-static bifurcation has the same directional solution with fractal uniformity and quasi-local stress components.

In a wide range the response of sand bodies to imposed deformations is *time-stretching invariant*. This means that the duration of driven stressing between jerks with microseismicity and flash-heating does not matter, although thermally activated inter-crystalline dislocations are rate-dependent (A1). Water-saturated sand is no more time-stretching invariant, although the grain fabric is so, if changes of pore volume entail a so rapid seepage that changes of pore water pressure matter for the fabric stress. This effect is negligible for a slow driven dilatation, but not for a collapse thereafter. Time-stretching invariance is also observed with rock samples (Sect. 4), and holds likewise with a wide range of overall stretching rates for lithosphere sections as outlined in the companion paper.

Analogue models with clay

Shear bands occur also in *water-saturated clay*, but clay particles are smaller and softer than sand grains. The permeability is far lower, therefore a driven evolution with dilating shear bands can turn the pore water pressure into suction ($p_w < 0$), and the rise of p_w by a collapse can last for a longer time. Thus shear box tests with water-saturated kaolin clay without overall drainage yield more detailed shear band patterns than with sand, this helps understand faults with Riedel shears (Morgenstern and Tchalenko 1967). A single shear band with about 10 clay particles thickness arises by shearing a thin layer of water-saturated clay, consolidated with up to 15 MPa, its shearing resistance has a low $\phi'_r \approx 10^0$ due to flat clay particles (Balthasar et al. 2006). As with sand, driven critical states of the clay fabric could be represented by saddle points of the elastic energy with regard to the elastic strain, and a collapse occurs at a tipping point with regard to the pore volume attained by dilatation.

Balthasar et al. (2006) report that a 3 mm thick clay layer under a constant overall pressure $\hat{\sigma} \approx 10$ MPa slightly below the previous consolidation pressure and a shear stress $\hat{\tau} > \hat{\sigma} \tan \phi'_r$ slid off after about 20 min. This collapse occurred after a quasi-static dilatation up to a critical pore volume in a shear band, delayed by the access of pore water and the rate-dependence of the mineral (A1). The subsequent shearing is enhanced by an increase of p_w as the excess pore water due to the sudden contraction could not evade in a short time. This mechanism helps explain the Vajont catastrophy 1963 (Hardenberg 2011): a part of the Monte Toc imposed nearly stationary $\hat{\sigma}$ and $\hat{\tau} > \hat{\sigma} \tan \phi'_r$ to an inclined mudstone layer, this dilated slowly up to a critical pore volume, then the mineral fabric collapsed so that p_w rose and the rock mass above slid down with acceleration. On the other hand, the fabric of clay smears in faults (Vrolijk et al. 2016) can relax so that their elastic energy does not attain a tipping point by tectonic stressing, but the dilatation can enhance the opening of clay smears and erosion.

Soil-like masses, and limitations

Soil-like masses without water are also used for tectonic analogue models (Rosenau et al. 2016). Viscoplastic masses with silicone are capable of shear localization, but without dilatation and micro-seismicity. Dry powder with a slight cohesion dilatates with shearing by widening of cracks, and can yield geometrical features of faults and cracks near the free surface (Holland et al. 2006). Such analogue models can reproduce features of tectonic critical phenomena with dilatancy both by shear banding and cracking, but not of spontaneous ones with contractancy and enhancement by pore water.

The localized dilatation and the subsequent contraction of grain fabrics, which occur analogously also in the lithosphere, elude a mathematical treatment with continuum

models and locally confined constitutive relations. Localized shearing can be analyzed by means of additional polar quantities, this can lead to a fractally uniform pattern within a stretched layer. The emergence of fractal patterns with dilatancy cannot generally be captured with systems of differential equations (as proposed e.g. by PELETIER AND TROY 2001) as spatial and temporal fractal distributions cannot be classically differentiated. Thus rearrangements of grain fabrics with fractal shear band patterns are not properly captured by classical stretching rate tensors. Deformations may be employed for samples in experimental devices, and also for technical structures embedded in the ground, but for lack of an objective reference configuration this notion is not adequate for the lithosphere. On the other hand, solutions of quasi-static bifurcation problems with quasi-local stress tensors can yield orientations of major shear bands which match orientations of shear bands in sand samples and main faults in the lithosphere despite the ever-present fractality.

The relation of quasi-local quantities with probabilities poses further problems. Mean values could be defined as mathematical expectations if underlying random sets were specified by probability distributions, but these are not given. The quasi-local specific configuration entropy $\hat{s}_\chi$, which is assumed proportional to $\hat{\chi}^2$ as implied by GUDEHUS' (2019) model without fractality, could be proportional to a Tsallis entropy s_T as a measure of disorder beyond Boltzmann's specific entropy s_B. SORNETTE (2000) shows that s_T is maximal for fractal random sets and turns into s_B without fractality. With a driven dilatant stressing $\hat{s}_\chi$ increases and the fractal exponent α decreases, thus the formation of fractal patterns means a growing disorder, while a contractant collapse in a chain reaction means a spontaneous regain of order. On the other hand, s_B decreases by a driven stressing and increases by a subsequent chain reaction, that's why the wax and wane of tectonic structures cannot be captured by thermodynamics only.

4 Analogue models with rock

Uniaxial and triaxial tests with sandstone

Changes of crystal lattice distances, observed in *uniaxially* loaded sandstone samples via the diffraction of neutron beams (FRISCHBUTTER et al. 2000), reveal a growing non-homogeneity of elastic strain alongside with growing cracks. Elastic strain and related stress are thus no more the ones in CAUCHY'S (1827) sense. These findings confirm that tectonic dislocations elude continuum approaches as fluctuation wavelengths diverge, whereas inter-crystallite dislocations of pore-free solids with locally confined fluctuations can be captured by a mean-field theory with locally confined fluctuations (A1). Like with sand, dislocations of rock with dilatancy therefore cannot be captured with materials science, thermodynamics and continuum mechanics. However, uniaxial tests with rock samples may be considered as *tectonic analogue models* as far as cracks dominate also in

situ. We turn now to triaxial tests which yield mainly shear bands, and a criterion for the distinction from dominant cracks will be proposed.

Water-saturated sandstone samples were repeatedly brought to limit states, visible by a sudden drop of the overall stress deviator $\hat{\sigma}_1 - \hat{\sigma}_3$, in *multi-stage triaxial tests* with axial shortening, controlled $\hat{\sigma}_3$ and/or pore water pressure p_w at an endplate (Lempp et al. 2020). Plots of peak $\hat{\sigma}_1 - \hat{\sigma}_3$ versus mean effective pressure $\hat{p}' \equiv (\hat{\sigma}'_1 + 2\hat{\sigma}'_3)/3$ for such states can be captured by a Mohr-Coulomb condition in the range $\hat{\sigma}'_3 > \hat{c}'$. The validity for various $p_w/\hat{\sigma}_3$ confirms Terzaghi's relation (2). Initially 'intact' samples have an effective peak friction angle $\phi'_p \approx 50^0$ and an effective cohesion $\hat{c}' \approx 15$ MPa. Subsequent limit states with higher $\hat{\sigma}'_3$, achieved without disintegration of the sample by means of a servo-control, can be captured with an almost undiminished ϕ'_p, while $\hat{c}'$ vanishes nearly in the 3rd or 4th stage. The modulus of elasticity $\hat{E}$ for un- and reloading increases less than linearly with $\hat{\sigma}'_3$ from its amount for $\hat{\sigma}'_3 \approx \hat{c}'$, and scatters like $\hat{c}'$.

Figure 1: Unrolled combined photographs of a cylindrical sandstone sample after a multi-stage triaxial test with $\hat{\sigma}'_3 > \hat{c}'$ except at the onset and near the endplates (Lempp et al. 2020)

Cylindrical sample surfaces, unwrapped after test stages with $\hat{\sigma}'_3 > \hat{c}'$, exhibit in the middle third fractally uniform patterns of shear bands with few cracks (e.g. Fig. 1). Like with sand the shear bands are inclined against $\hat{\sigma}'_1$ by $\theta \approx \pm(45^0 - \phi'/2)$. Cracks - opened by complete unloading - follow shear bands, whereas cracks percolating the whole sample dominate in experiments with $\hat{\sigma}'_3 < \hat{c}'$. The repeated quasi-static widening of shear bands with minute cracks means a *driven dilatation*. The reduction of $\hat{\sigma}_1 - \hat{\sigma}_3$ thereafter with

constant $\hat{\sigma}_3$ entails a *spontaneous contraction*, which is indicated by a crackling noise and a temporary increase of p_w. The contraction of shear bands is accompanied by a comminution of grains.

The response of the solid fabric in driven test stages is *time-stretching invariant*, i.e. the velocity of shortening - including rest intervals - does not matter for changes of $\hat{\sigma}'_1$ and $\hat{\sigma}'_3$, nor for the overall pore volume fraction $\hat{n}$, with the overall axial strain $\hat{\epsilon}_1$. This happens as the duration of thermally activated dislocations is far shorter than the one of quasi-static driving intervals (A1). However, driving stages exhibit *jerks* of different size, i.e. brief local losses of equilibrium and a stabilization thereafter without an overall collapse. The flash-heating of dry rock samples, observed with up to 1650^0 C by Brady and Rowell (1986), indicates that inter-crystalline dislocations can be up to about 10^{14} times faster than overall deformations of the porous solid (like with sand, Sect. 3). The time-stretching invariance is thus delimited by thermally activated dislocations, but even with elevated temperatures they do not matter in triaxial tests with hard mineral and attainable duration.

Uniaxial and triaxial tests with granite

Uniaxial and triaxial tests have also been carried out with *water-saturated granite* samples at 200^0 to 300^0 C (Lempp 1994). Taken from quarries, they had minute inter-connected cracks with an overall pore volume fraction $\hat{n} \approx 0.002$ to 0.004. The overall permeability was initially low, viz. $\hat{k}_f \approx 10^{-14}$ m/s, but increased substantially by dilatation so that $p_w \approx 0$ was achieved with open drainage and a slow drive (negligible evaporation via narrow access tubes). Peak stress circles of originally 'intact' samples have a tangent with $\phi'_p \approx 40^0$ to 45^0 and $\hat{c}' \approx 20$ to 30 MPa. $\hat{c}' \approx 0$ was attained after four to five overall losses of equilibrium, confined by a servo-control, while ϕ'_p decreased scarcely and $\hat{n}$ increased up to about 0.006 to 0.012. Tests without drainage led to lower ϕ and higher $\hat{c}$ with total stress components $\hat{\sigma}_1$ and $\hat{\sigma}_3$ due to higher p_w, but the latter could not be observed (nor with direct shear tests) so that the entailed reduction of $\hat{p}'$ can only be guessed.

The initial modulus $\hat{E}$ for uniaxial reloading is approximately proportional to the uniaxial compressive strength $\hat{\sigma}_d$ of intact samples, with the same factor for different granites (Lempp and Natau 1985). Lower overall void ratios $\hat{e} \equiv \hat{n}/(1+\hat{n})$ are related with higher $\hat{\sigma}_d$. Shear tests with faults of the same granite yield ϕ_p from about 30^0 to 40^0, residual ϕ_r from about 25^0 to 30^0 and c from zero to about 0.8 MPa.

Keeping the total axial stress constant the sample got shorter within several weeks, and keeping the sample height constant the axial stress decreased and partly returned, both with *jerks* and rest intervals of few days (Fig. 2). Despite higher temperatures this

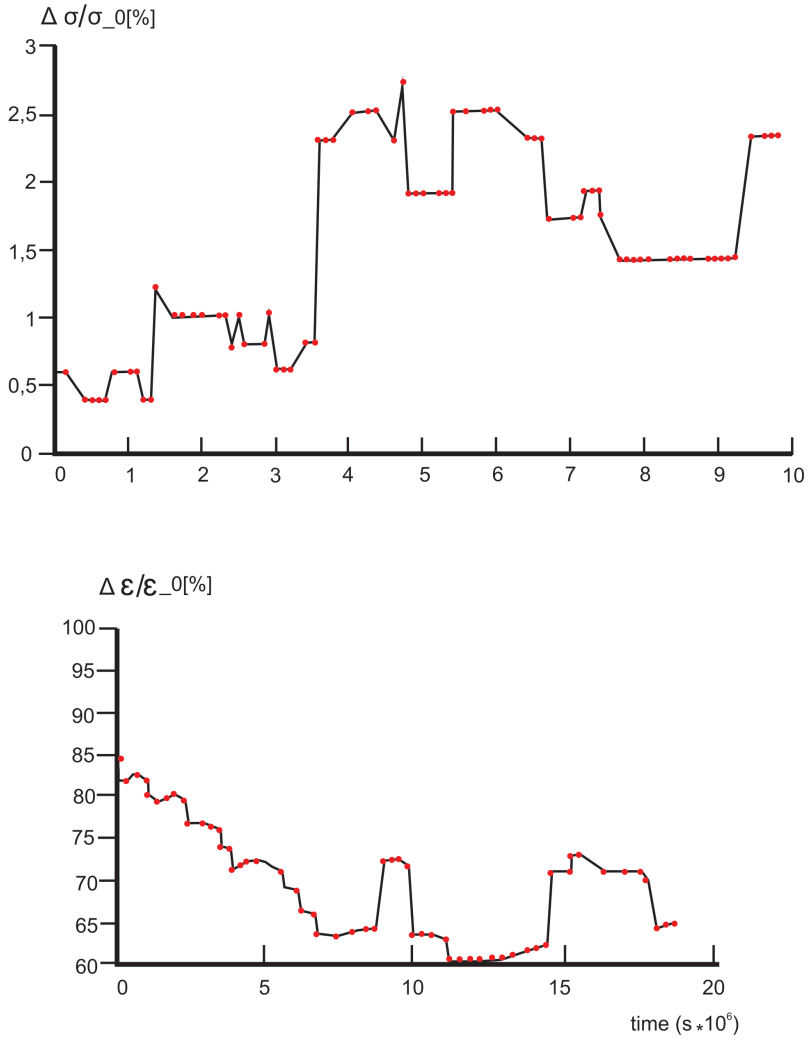

Figure 2: Jerky relative changes of axial strain with constant stress (above) and stress with constant height (below) of water-saturated granite samples in uniaxial tests (after Lempp 1994). ϵ and σ denote axial shortening and pressure, respectively, subscript 0 denotes their onset values and Δ autogeneous changes, times in 10^6 seconds

behavior cannot be explained with thermally activated dislocations as these would yield a smooth increase of $\hat{\epsilon}_1$ or decrease of $\hat{\sigma}_1$, respectively, in far longer times (A1). The jerks indicate fractal fluctuations like with sandstone, therein rest intervals enable a diffusion of pore water as outlined further below.

Crystallites of granite had sizes up to about 2 mm, therefore shear bands with about ten grains thickness could not evolve in patterns like with our fine-grained sandstone. Only

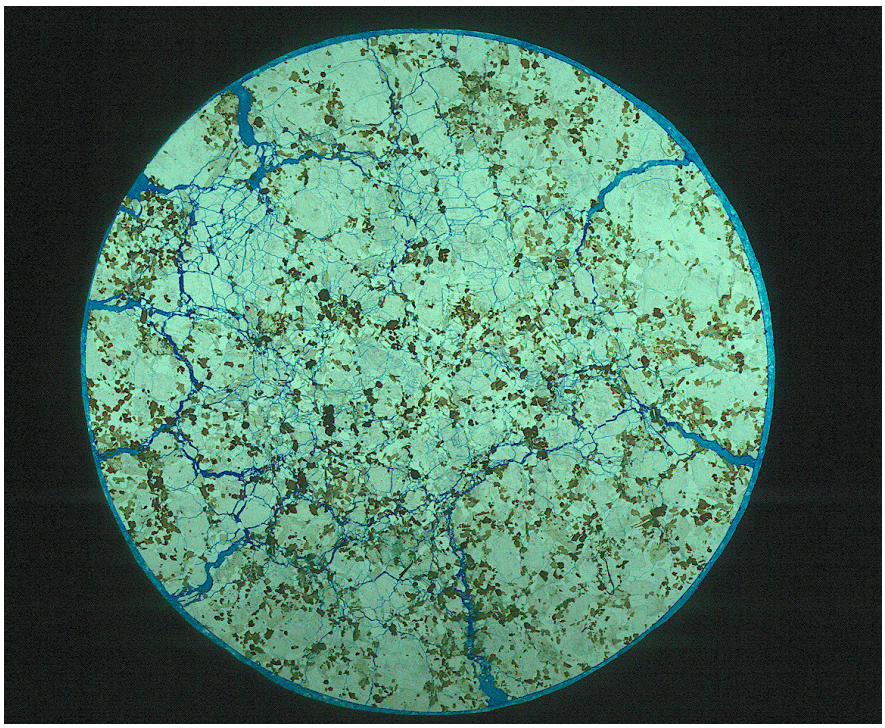

Figure 3: Section of a granite sample at mid-height after a triaxial test with $\hat{\sigma}'_3 < \hat{c}'$, pore system filled with epoxy resin (ALTHAUS et al. 1994)

a single shear band arose from top to bottom in tests with $\hat{\sigma}'_3 > \hat{c}'$, its inclination against $\hat{\sigma}'_1$ was roughly $45^0 - \phi'/2$. Polished horizontal sections of granite samples after tests with $\hat{\sigma}'_3 < \hat{c}'$ exhibit a *fractal non-uniformity* (e.g. Fig. 3). Major nearly radial primary cracks dwindle towards the centre, secondary cracks branch from the primary ones, tertiary ones can scarcely be identified among cracks of the initially 'intact' sample. Such cracks arise in a hierarchical succession of bifurcations during which the pore volume increases, though with a waning amount towards the centre for lack of freedom there. This kind of non-uniformity resembles the one of shear band patterns of sandstone samples after tests with $\hat{\sigma}'_3 > \hat{c}'$ (Fig. 1), and the latter can likewise be attributed to *hatched successive bifurcations* which are characteristic of fractality (Mandelbrot 1982). Its confinement by the endplates and the rubber membrane causes non-fractal gradients of mechanical quantities which can be reconciled with the fractal non-differentiability by means of quasi-local quantities and fractional gradients (Appendix A2). In the sequel we will first

take overall quantities instead of quasi-local ones and then take into account non-fractal gradients, though in a simplified way. Fractional gradients are employed analytically in the companion paper.

Constitutive relations

Like with sand the frictional resistance of rock results from repulsive solid bridges and dilatancy. Both factors would not occur without a pore system as the mineral is nearly incompressible, they determine the shearing resistance even with a minute pore volume and are more pronounced than along smoothed-out faults. The effective cohesion $\hat{c}'$ can be attributed to *cohesive solid bridges* which entail an additional fabric pressure $\hat{p}_c$ so that the fabric stress components are $\hat{\sigma}_1^f = \hat{\sigma}_1' + \hat{p}_c$ and $\hat{\sigma}_3^f = \hat{\sigma}_3' + \hat{p}_c$. For simplicity the additional pressure is thus assumed isotropic, this suffices for judging critical phenomena with dominating shear bands for $\hat{\sigma}_3' > \hat{c}'$, but not those with dominating cracks for $\hat{\sigma}_3' < \hat{c}'$. $\hat{p}_c$ means $\hat{c}' = \hat{p}_c \tan\phi'$, i.e. $\hat{c}' \approx \hat{p}_c$ for $\phi' \approx 45^0$. While ϕ' rises by dilatancy $\hat{p}_c$ dwindles and can disappear, thereafter the fabric has only repulsive bridges. This approach substitutes the one by Griffith (1922) for a single crack, and also the one by Vardoulakis and Sulem (1995) without fractality. Leaving first aside multi- and non-fractal trends by endplates and radial symmetry, we employ overall quantities of the sample instead of quasi-local ones (A2), denoting both by $\hat{}$.

Our constitutive model for sand (A3) is extended for rock in Appendix A4. In addition to the elastic energy $\hat{w}_e$ the potential energy has a term $\hat{w}_c$ for cohesive bridges, this is the potential of $\hat{p}_c$ via their strain $\hat{\epsilon}^c$ which is related with the volumetric strain of the fabric, thus $\hat{\sigma}_1^f = \hat{\sigma}_1' + \hat{p}_c$ and $\hat{\sigma}_3^f = \hat{\sigma}_3' + \hat{p}_c$ are obtained. The fabric is dilatated by axial shortening with constant $\hat{\sigma}_3'$, this means a driven succession of saddle points of $\hat{w}_e$ and tipping points of $\hat{w}_c$ so that ϕ' grows, while $\hat{p}_c$ wanes alongside with the specific area $\hat{s}_c$ of cohesive bridges. Like with sand the dilatation ends with a collapse of the fabric when its energy $\hat{w}_e$ attains a tipping point with regard to the pore volume fraction $\hat{n}$. The collapse entails a contraction, i.e. a reduction of $\hat{n}$, which is delayed by the pore water, and a drop of $\hat{\sigma}_1'/\hat{\sigma}_3'$, in the case of axial shortening which implies $\hat{\sigma}_3' > \hat{c}'$.

Incorporating the pressure $\hat{p}_c$ from cohesive bridges, driven successions of saddle points with radial symmetry can be captured by the *extended stress-dilatancy relation*

$$\frac{\hat{\sigma}_1^f}{\hat{\sigma}_3^f} \equiv \frac{\hat{\sigma}_1' + \hat{p}_c}{\hat{\sigma}_3' + \hat{p}_c} = -2\tan^2(\pi/4 + \phi_r'/2)\frac{d\hat{\epsilon}_3^i}{d\hat{\epsilon}_1^i}. \tag{5}$$

It is confirmed by triaxial tests with sandstone, e.g. Fig. 4. Therein $\hat{\sigma}_1'/\hat{\sigma}_3'$ and $d\hat{\epsilon}_3/d\hat{\epsilon}_1$ are calculated by combining smoothed-out plots of $\hat{\sigma}_1'$ and $\hat{\epsilon}_3 = 2\hat{\epsilon}_v - \hat{\epsilon}_1$ versus $\hat{\epsilon}_1$, wherein the

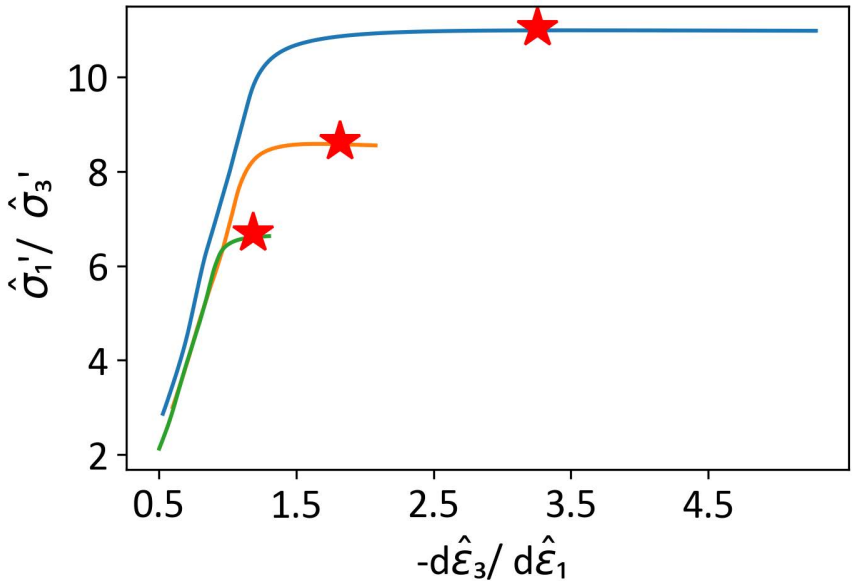

Figure 4: Stress-dilatancy plots of a water-saturated sandstone sample in a triaxial test with $\hat{\sigma}_3' = 9$ to 11 MPa in the second (upper), third (middle) and fourth (lower curve) driven stage up to a spontaneous drop (asterisk) of $\hat{\sigma}_1' - \hat{\sigma}_3'$ (Menezes 2022)

volumetric strain $\hat{\epsilon}_v$ is determined by volume changes of pore water as directly measured $\hat{\epsilon}_3$-values are not reliable (Menezes 2022). $d\hat{\epsilon}_3^i/d\hat{\epsilon}_1^i$ as in (4) is replaced by $d\hat{\epsilon}_3/d\hat{\epsilon}_1$ for simplicity, which is legitimate as elastic fractions are below 1/10 of total strain increments. $\hat{p}_c = 0$ (i.e. $\hat{c}' = 0$) is nearly attained in the 4th stage, then (5) reduces to (4) so that ϕ' grows from 31^0 (no dilatancy) to 50^0 (maximal dilatancy). The plateau of $\hat{\sigma}_1'/\hat{\sigma}_3'$ for the 2nd stage leads to $\hat{p}_c \approx 9$ MPa with the same ϕ', this matches $\hat{c}' = \hat{p}_c/\tan 50^0 \approx 10$ MPa as obtained for the 1st stage. Values of $\hat{\sigma}_1'/\hat{\sigma}_3'$, increased by $\hat{p}_c$, enable a calibration of $\hat{p}_c$-parameters (A4), but these are not needed in the sequel.

The curves in Fig. 4 cannot be captured by (5) near the plateau, and this formula fails also for $\hat{\sigma}_3' < \hat{c}'$ as then cracks dominate (Menezes 2022). Minute cracks open near the endplates despite $\hat{\sigma}_3' > \hat{c}'$ with overall quantities as there shear bands cannot arise (cf. Fig. 1) and $\hat{\sigma}_3'$ gets lower than $\hat{c}'$. A more precise distinction by the sign of $\hat{\sigma}_3' - \hat{c}'$ requires quasi-local quantities as overall quantities get insufficient substitutes with a growing fractal non-uniformity (A2). For test stages with dominant shear bands the dwindling $\hat{c}'$ has about the same spatial fluctuation as $\hat{\sigma}_1'$ and $\hat{\sigma}_3'$, this speaks for (5) in the range $\hat{\sigma}_3' > \hat{c}'$.

The *collapse* after a peak of $\hat{\sigma}_1' - \hat{\sigma}_3'$ versus $\hat{\epsilon}_1$ (confined by the servo-control) ensues an inelastic contraction, i.e. $d\hat{\epsilon}_1^i + 2d\hat{\epsilon}_3^i > 0$, which means a reduction of the volumetric

elastic strain $\hat{\epsilon}_v^e \equiv \hat{\epsilon}_1^e + 2\hat{\epsilon}_3^e$, and therefore of the effective pressure $\hat{p}' \equiv (\hat{\sigma}_1' + 2\hat{\sigma}_3')/3$, as the initial volume increment is $d\hat{\epsilon}_1 + 2d\hat{\epsilon}_3 = 0$ due to the incompressibility of mineral and pore water. Repeated collapses occurred at $\hat{n} \approx 0.11$ in the test of Fig. 4, despite the non-uniform porosity this confirms our assumption that a loss of equilibrium occurs at a tipping point of the elastic energy $\hat{w}_e$ with regard to $\hat{n}$.

Biaxial tests

Biaxial tests with rock samples between two smooth plates like with sand, which yield shear band patterns up to a dominating band (Sect. 3), are not available with rock. Biaxial devices with cubical rock samples fixed at their corners (e.g. Li et al. 2021) yield patterns of shear bands and cracks which exhibit no analogy with the lithosphere, and elude also methods of materials science. However, experimental setups with perforated rock blocks between two fixed hard and smooth plates can serve as biaxial analogue models, not only for estimating in situ stresses from borehole logging data. Lempp et al. (2012) loaded a sandstone block with an included steel tube in such a device. The orientation of the achieved ovalization of the tube matched the anisotropy of the imposed external stress components. After a test the block exhibited dilatancy with dominant shear bands and minor cracks, which was more marked towards the perforation. The thus indicated coaxiality of quasi-local stress and stretching rate tensors matches the principle of maximal dissipation, which supports also our stress-dilatancy relation (Appendix A4).

The stress at the block's surface, calculated with isotropic elasticity and the stress at the tube from its elastic deformation, is about half the imposed external stress (Lempp et al. 2012). The difference can be explained by means of our constitutive model (A3 and A4). The second term of the evolution equation (14) of elastic strain is negligible against the first one as $\hat{\chi}$ is below 100 and $\hat{\epsilon}_i^e$ below 10^{-4}. The resulting relation $d\hat{\epsilon}_i^e = (1 - \hat{\mu})d\hat{\epsilon}_i$, with $1 - \hat{\mu}$ from about 0.3 to 0.7 for a driven dilatation, means that the elastic strain increment $d\hat{\epsilon}_i^e$ is about half the total one $d\hat{\epsilon}_i$. Calculated stress increments are likewise underestimated as the incremental elasticity by (12) is nearly isotropic and the modulus E is nearly constant by (16). Thus the observed underestimation of the external stress without inelastic effects confirms our theory, and with it such biaxial tests are of use beyond borehole logging.

Interaction of solid fabric and pore water

After a sudden rise of $\hat{p}_w$ in the range $\hat{\sigma}_3' > \hat{c}'$ the contraction of the pore system can go on with seepage until a new equilibrium is attained with the pre-collapse p_w and $\hat{p}'$, but lower deviator $\hat{\sigma}_1' - \hat{\sigma}_3'$ and surface $\hat{s}_c$ of cohesive bridges. In other words, after a slow stressing and dilatation a collapse with dominant shear bands causes a temporary rise of pore water pressure, and leaves back a denser fabric with a lower stress deviator and

a reduced cohesion. Both dilatation and contraction are captured by our constitutive model, also beyond axial symmetry (A4). Thus calculated speeds of P- and S-waves match the ones observed in triaxial tests and in situ (GUDEHUS et al. 2022).

The entailed *hydraulic diffusion*, i.e. the autogeneous interaction of seepage and nearly elastic change of pore volume, causes a delay of the contraction by

$$\hat{t}_d \approx d^2 \frac{\gamma_w}{\hat{k}_f \hat{E}} \tag{6}$$

with sample size d, specific weight γ_w of water, Young's modulus $\hat{E}$ and permeability $\hat{k}_f$. $\hat{t}_d$ by (6) denotes the time for a water-saturated poro-elastic solid to reach an equilibrium after imposing and keeping constant a total pressure (GUDEHUS 2011). This is a crude estimate as the seepage of water is not properly captured by Darcy's law with a fractal pore system: like the motion of the rock fabric the one of pore water is not temporally and spatially differentiable, but it could be captured with fractional derivatives (Appendix A1 of the companion paper). With $\gamma_w \approx 10$ kN/m^3, $d \approx 0.1$ m, $\hat{E} \approx 10^7$ kPa and $\hat{k}_f \approx 10^{-9}$ m/s (6) yields $\hat{t}_d \approx 100$ s for sandstone, less with wider cracks and more for granite as visible e.g. in Fig. **??**.

Imagine a subdivision of the sample into smaller inspection cubes, say with 1 cm width for a sample diameter of 10 cm so that there are about 1000 cubes. Pore system and elastic strain components for each of them may be observed via attenuation of X-rays and diffraction of neutron beams, respectively (GUDEHUS et al. 2022). These data could be evaluated for getting quasi-local quantities and non-fractal trends. If a loss of equilibrium occurs in a cube its pore water pressure increases and a part of its elastic energy turns into kinetic energy. Thus generated seismic waves and hydraulic diffusion enhance an audible *seismogenic chain reaction*, which comes to an end with less critical surrounding cubes or by the servo-control for the sample as a whole.

Limitations

Differently to limitations for tectonic analogue models with soil-like matter (Sect. 3), those with rock samples are of limited validity also due to cracks. The proposed distinction of dominant shear bands or cracks by the sign of $\hat{\sigma}'_3 - \hat{c}'$ is imprecise as both the quasi-local effective cohesion $\hat{c}'$ and the smallest principal stress $\hat{\sigma}'_3$ can but crudely be estimated. Plots of axial stress and volumetric strain versus axial strain can be smoothed out for the range with $\hat{\sigma}'_3 > \hat{c}'$ as fluctuations in the sample are confined by its boundary conditions, while an analogous restriction in lithosphere sections is less evident. A rockburst in the range $\hat{\sigma}'_3 < \hat{c}'$ would be dilatant, and a single crack can arise with $\hat{\sigma}'_3 = 0$

(axial splitting) or $\hat{\sigma}'_1 = 0$ (discing). Apart from rockburst the proposed relations of quasi-local and -momentary quantities imply a power-law dependence on the size of inspection cubes except the coefficient of variation, but cannot reproduce the formation of fractal patterns more in detail. A configuration entropy, as outlined at the end of Sect. 3, could lead to probability distributions for this kind of fractality.

5 Conclusions and outlook

We explain the slow tectonic widening of shear bands (faults) with minor cracks as quasi-static driven succession of critical points of porous solid fabrics within fractally uniform inspection cubes, which are suitably chosen for analogue models of the lithosphere. Therein the fabric state is described by quasi-local mean values of elastic strain and energy-conjugated stress, pore volume fraction, specific surface of cohesive solid bridges, and an eutaraxy (sensitivity) which is proportional to the coefficient of variation of spatial fluctuations. During a driven dilatation of the fabric its elastic energy is at saddle points with regard to its elastic strain, while the potential energy of cohesive bridges is at tipping points. Such successive critical points can equivalently be represented by a Mohr-Coulomb condition with an increasing friction angle by dilatancy and a waning cohesion by opening cohesive bridges.

This evolution is captured by a stress-dilatancy relation including the effective cohesion $\hat{c}'$, which is validated by triaxial tests with water-saturated sandstone samples. This relation works as long as the dilatation is mainly localized in shear bands and not in cracks, which requires that the smallest principal effective stress $\hat{\sigma}'_3$ exceeds the effective cohesion $\hat{c}'$ in a quasi-local sense. It implies a maximal rate of dissipation, which justifies also the coaxiality of stress and stretching rate tensors, and includes an angle near $45^0 - \phi'/2$ between $\hat{\sigma}'_1$ and shear bands. Quasi-local and -momentary quantities are mean values of inspection cubes which depend on its size except the coefficient of variation, and are legitimate although a driven dilatation proceeds with jerks. With the prevailing hard minerals the reaction to a drive is largely time-stretching invariant. The drive is enhanced by an injection of pore water, while the pore water pressure is not reduced by a slow driven dilatation with an open drainage.

A dilatated fabric collapses with contraction when its elastic energy attains a tipping point with regard to the pore volume fraction. The contraction is impeded by the pore water until a part of it flows towards a less critical surroundings. As far as the latter is nearly collapsible and equally aligned a collapse front widens laterally by pressure waves and proceeds by the spreading of pore water in a mechanical chain reaction. Such spontaneous critical phenomena entail a stress-drop and a contraction of the solid fabric, thereafter a continued drive leads again to dilatation and stressing up to a collapse, and so on with with diverging fluctuation wavelengths. This concept works as long as shear

bands dominate in the range where the the smallest principal effective stress exceeds the effective cohesion in a quasi-local sense. Otherwise cracks dominate, and widen also beyond a tipping point of the quasi-local elastic energy with regard to the pore volume fraction so that the collapse is dilatant.

As shown in the companion paper these features are scale-independent, and they could be further investigated with triaxial and model tests. Micro-seismicity, attenuation of X-rays and diffraction of neutron beams could help clarify fractal features of pore system and solid fabric so that quasi-local and -momentary state variables are better understood (Gudehus et al. 2022). State variables could be extended with further invariants and directional features, thus constitutive relations could be sophisticated. Successions of driven and spontaneous critical phenomena with dilatancy and contractancy, respectively, could be captured by an extended field theory with fractional rates and gradients. The implied probability distributions could be captured by means of a configuration entropy in addition to Boltzmann's entropy. The rockburst, which is a dilatant collapse with a waning stress deviator, can lead to a dominant single crack instead of a dominant shear band. Other critical phenomena, especially folding and convection cycles, could similarly be taken into account in analogue models and their evaluation. These could replace numerical simulations, which are not classically legitimate for lack of differentiablity, although boundary conditions in the lab are simpler than with lithosphere sections.

APPENDIX

A1 Thermally activated dislocations

Persson (2000a) considers dislocations of a pore-free solid with crystallites and thermal oscillation. Employing Maxwell's normal distribution for spatially confined scattering, he derives the relationship

$$\sigma = 2c_d[1 + \frac{k_B T}{E_a} \ln(\frac{3G}{c_d} \frac{E_a}{k_B T} \frac{\dot{\epsilon}}{f_c})] \tag{7}$$

of deviatoric stress σ and strain rate $\dot{\epsilon}$ for one-dimensional stretching in the range

$$\exp(\frac{-E_a}{k_B T}) \ll \frac{3G}{c_d} \frac{E_a}{k_B T} \frac{\dot{\epsilon}}{f_c} \ll 1 \tag{8}$$

with absolute temperature T, Boltzmann constant k_B, shear modulus G, crystalline shear strength c_d, activation energy E_a and a reference frequency f_c. Assuming $E_a \approx c_d d_d^3$ for nano-sized blocks of length d_d and cohesion c_d, and $f_c \approx c_s/d_d$ with speed c_s of shear

waves, the evaluation of creep tests with steel yields $E_a/k_BT \approx 40$, which means $E_a \approx 5$ eV (electron volt) with 1 eV$\approx 40k_BT$ for $T = 293$ K. With these data and $3G/c_d \approx 10^3$ the lower bound in (8) means roughly $\dot{\epsilon} \gg 10^{-9}$/s, under it the relation of σ with $\dot{\epsilon}$ gets linear so that $\sigma \to 0$ is obtained for $\dot{\epsilon} \to 0$. The upper bound means roughly $\dot{\epsilon} \ll 10^{10}$/s, over it mechanical heating reduces σ.

A2 Fractality and fractionality

Taking over MANDELBROT'S (1982) mass fractal, the solid mass of a fractal solid within iso-centric cubes of width d is $m = m_r(d/d_r)^{3\alpha}$ with an exponent α just below 1. Equivalently, the added-up solid mass length along a straight line is proportional to $(d/d_r)^\alpha$. The implied fractal uniformity holds for d from a lower bound d_r up to an upper bound, therein the mass density is $\hat{\rho} = \rho_r(d/d_r)^{3(\alpha-1)}$. The elastic energy and its density $\hat{w}_e$ depend likewise on d, and via (18) also the mean solid pressure $\hat{p}'$, while the direction $\hat{\sigma}'_{ij}/|\hat{\sigma}'_{ij}|$ of effective stress is d-independent. α just below 1 results from a slightly higher fraction of wider faults and cracks within wider cubes, but α can scarcely be calculated from in situ data. α varies spatially and temporally as it evolves with reconfigurations (A3 and A4), lower amounts indicate a more marked fractality.

With temporal fractality the seismic velocity v at a point has a spectrum $v^2 \propto f^{-2\beta}$ with β just below 1 within lower and upper bounds of frequency f. Observed spectra do not enable a precise determination of β, and the ensued reduction of $v^2/\Delta t$ with a longer observation interval Δt by a factor $\propto (\Delta t)^{\beta-1}$ can only be postulated. The simplifying assumption $\beta = \alpha$ is justified by observed features of wave propagation (GUDEHUS AND TOUPLIKIOTIS 2016). The lowest duration t_r of intervals with stationary fractality may be related with d_r by $t_r = d_r/v_d$ with a relative driving velocity v_d.

The fractional derivative $d^\alpha f/dx^\alpha$ (shorthand instead of a convolution integral) of a function $f(x)$ is the average of difference quotients for sections of length $\Delta x = \xi x_r$ around x with weighting factor $1/\xi^\alpha$ and reference length x_r. $d^\alpha f/dx^\alpha = 0$ leads to $f \propto (x/x_r)^\alpha$ (TARASOV 2005), this means fractal uniformity as proposed above with the same exponent α. The fractional gradient $\nabla_{ij} f(x_i, t)$ of a function $f(x_i)$ is defined analogously for three coordinates x_i. The temporal fractional derivative $d^\beta g/dt^\beta$ of a function $g(t)$ is likewise defined, but one-sided for causality. With $\alpha = \beta$ the temporal partial fractional derivative is $\partial^\alpha f(x_i, t)\partial t^\alpha$, while the reference quantities $x_r = d_r$ and t_r can be defined and related as outlined above. Thus a displacement $u_i(x_i, t)$ leads to a velocity $v_i = \partial^\alpha u_i/\partial t^\alpha$ and a stretching rate $D_{ij} = (\nabla^\alpha_{ij} v_j + \nabla^\alpha_{ij} v_j)/2$.

Balances of conserved extensive quantities - mass, energy and momentum - are expressed by fractional integrals, and can be translated into fractional differential equations. TARASOV (2005) proposed a fractional divergence theorem which relates spatial integrals and

boundary conditions, but assumed a temporal $\beta = 1$. Temporal integration with ca $0.9 < \beta = \alpha < 1$ requires an initial condition which is not easily given. The Fourier transform of $d^\alpha f/dx^\alpha$ is $\alpha f(x)$, with $f(x_i)$ this leads to a triple transform integral. The one-sided Laplace transform of $d^\beta g/dt^\beta$ is $\beta g(t)$. A quantity $f(x_i, t)$ with fractional derivatives may be interpreted as mathematical expectation $\hat{f}(x_i, t)$ of a fractal random set in a quasi-local and -momentary sense. The eutaraxy $\hat{\chi}$, which is related with $\alpha = \beta$, is proportional to the coefficient of variation in our constitutive approach (A3 and A4), so it does not depend on size and duration of inspection cubes and intervals, respectively, in the case of fractal uniformity and stationarity.

A3 Constitutive relations of sand with fractality

In an elastic range the total differential of mechanical work per unit of volume of a homogeneous grain fabric would be

$$dw = \sigma'_{ij} d\epsilon_{ij} = dw_e = \sigma'_{ij} d\epsilon^e_{ij} \tag{9}$$

if there were no spatial fluctuations beyond those by inter-crystalline dislocations (A1). (9) would lead to (3) with $\mu = 0$. Extending Gudehus' (2019) theory to a fractally homogeneous inspection cube of sand with shear bands, its quasi-local elastic energy can be represented as

$$\hat{w}_e = B\hat{\epsilon}^e_v(\hat{\epsilon}^{e2}_v + b\hat{\epsilon}^{e2}_d) \tag{10}$$

with quasi-local volumetric and deviatoric invariants $\hat{\epsilon}^e_v \equiv \hat{\epsilon}^e_{ii} > 0$ and $\hat{\epsilon}^e_d \equiv |\hat{\epsilon}^e_{ij} - \hat{\epsilon}^e_v \delta_{ij}|$. Therein b depends on the quasi-local pore volume fraction $\hat{n}$ by

$$b = b_p - (b_p - b_0)(\frac{\hat{n}_p - \hat{n}}{\hat{n}_p - \hat{n}_0})^2 \tag{11}$$

with peak and reference values $b = b_p$ for $\hat{n} = \hat{n}_p$ and $b = b_0$ for $\hat{n} = \hat{n}_0$. Saddle points of $\hat{w}_e$ have $\hat{\epsilon}^e_d/\hat{\epsilon}^e_v = \sqrt{2/b}$, which means $\hat{\tau}/\hat{p}' = \sqrt{2b}$ with the mean fabric pressure $\hat{p}' \equiv \hat{\sigma}'_{ii}/3$ and the deviatoric stress invariant $\hat{\tau} \equiv |\hat{\sigma}'_{ij} - \hat{p}'\delta_{ij}|$ by

$$\hat{\sigma}'_{ij} = (1 - \hat{\mu})\frac{\partial \hat{w}_e}{\partial \hat{\epsilon}^e_{ij}} \tag{12}$$

instead of (3). $\hat{\mu}$ is related with the quasi-local eutaraxy $\hat{\chi}$ by $\hat{\mu} = \hat{\mu}_h\hat{\chi}/\hat{\chi}_h$, wherein h denotes the hypoplastic range. $\hat{w}_e$ has a further critical point by (11), namely a tipping point at $\hat{n} = \hat{n}_p$. $G \approx \sqrt{B\hat{p}'}$ is obtained with (10) and (12) for the shear modulus G at $\hat{\tau} = 0$, which matches observations with $B \approx 100$ GPa for quartz sand at $\hat{n} = \hat{n}_{min}$. The friction factor b in (10) can be expressed by a friction angle ϕ', viz.

$$b = 6(\frac{\sin\phi'}{3 - \sin\phi'})^2, \tag{13}$$

for axial shortening of a cylindrical sample. Quartz sand has $\phi' \approx 30^o$ for a loose fabric and $\phi' \approx 40^o$ for a dense fabric with few shear bands, i.e. $b \approx 0.5$ and $b \approx 5$, respectively.

Taking over Gudehus' (2019) equations, driven evolutions of cylindrical inspection volumes can be captured by

$$d\hat{\epsilon}^e_i = (1 - \hat{\mu})d\hat{\epsilon}_i - \hat{\chi}[\hat{\epsilon}^e_i - h\hat{\epsilon}^e_v]d\hat{\epsilon} \tag{14}$$

for elastic and total overall strain increments, viz. $d\hat{\epsilon}^e_i, d\hat{\epsilon}_i$ and $d\hat{\epsilon} \equiv \sqrt{d\hat{\epsilon}_1^2 + 2d\hat{\epsilon}_2^2}$ for cylindrical symmetry (i=1, 2=3), with $h \approx 0.1$. The eutaraxy $\hat{\chi}$ evolves with deformations approximately by

$$d\hat{\chi} = \frac{c_\chi}{1 + \tan^2(\pi\hat{\chi}/2\hat{\chi}_h)}d\hat{\epsilon} \tag{15}$$

with $\hat{c}_\chi \approx 10^4$ and $\hat{\chi}_h \approx 100$ for monotonous drives. Including (12) with $\hat{\mu} = \hat{\mu}_h\hat{\chi}/\hat{\chi}_h$, the ratio $d\hat{\epsilon}^i_3/d\hat{\epsilon}^i_1$ of inelastic strain increments by (14) and (15) is independent of $\hat{\chi}$, whereas the differential of dissipated energy $d\hat{w}_d = \hat{\sigma}'_1 d\hat{\epsilon}^i_1 + 2\hat{\sigma}'_3 d\hat{\epsilon}^i_3$ is proportional to $\hat{\chi}$ and maximal for $d\hat{\epsilon}^i_3/d\hat{\epsilon}^i_1$ by the stress-dilatancy relation (4). The latter results from the maximum of $d\hat{w}_d = [\hat{\sigma}'_1 + 2\hat{\sigma}'_3 g(d\hat{\epsilon}^i_3/d\hat{\epsilon}^i_1)]d\hat{\epsilon}^i_1$ for g =const and $d^2g/d(d\hat{\epsilon}^i_3/d\hat{\epsilon}^i_1)^2 > 0$. (4) enables a calibration of the parameters in (11) with (13). The reduction parameter $\hat{\mu}$ can be related with the fractional exponent α by $\hat{\mu} = \hat{\mu}_h - (\alpha - \alpha_h)^2/(1 - \alpha_h)^2$ for capturing the actual multi-fractality.

(14) and (15) can be generalized, this leads to an invariant version of (4) and to coaxiality of $\hat{\sigma}'_{ij}$ or $\hat{\epsilon}^e_{ij}$ with quasi-local and -momentary stretching rates $\hat{D}_{ij}, \hat{D}^e_{ij} \equiv \dot{\hat{\epsilon}}^e_{ij}$ and $\hat{D}^i_{ij} \equiv \hat{D}_{ij} - \hat{D}^e_{ij}$ (A2). The dilatant evolution ends at a tipping point of $\hat{w}_e$ with regard to $\hat{n}$, thereafter $\hat{w}_e$ and $\hat{\tau}/\hat{p}'$ drop suddenly. This follows from (10), (11) and the generalization of (14) and (15). The evolution of $\hat{\chi}$ with rearrangements of the grain fabric

can be captured so that it ranges from 0 after a densification with minute cycles to $\hat{\chi}_h$ in the hypoplastic range. The latter holds for critical phenomena, then the coefficient of variation is also maximal. Presumably the latter is proportional to $\hat{\chi}$, and independent of the size of inspection cubes within fractal uniformity (A2), which is characteristic of fractality.

A4 Constitutive relations of rock with fractality

Modifying (10), the specific potential energy of fractally uniform parts of rock samples can be represented by

$$\hat{w} = \hat{w}_e + \hat{w}_c = B(\hat{\epsilon}_v^e)^{2/3}(\hat{\epsilon}_v^{e2} + b\hat{\epsilon}_d^{e2}) + C\hat{s}_a[(\hat{\epsilon}^c - \hat{\epsilon}_0^c) - \frac{(\hat{\epsilon}^c - \hat{\epsilon}_0^c)^2}{2(\hat{\epsilon}_c^c - \hat{\epsilon}_0^c)}] \tag{16}$$

with a fabric term $\hat{w}_e$ and an additional term $\hat{w}_e$ for cohesive bridges. $\hat{w}_e$ depends on volumetric ($\hat{\epsilon}_v^e > 0$) and deviatoric ($\hat{\epsilon}_d^e$) invariants of the quasi-local elastic fabric strain $\hat{\epsilon}_{ij}^e$ with a friction factor b by (11) and a stiffness factor B almost as by (10), but with $(\hat{\epsilon}_v^e)^{2/3}$ instead of $\hat{\epsilon}_v^e$ for capturing the observed increase of the modulus E of axial stiffness with uniaxial strength and confining pressure. $\hat{\epsilon}^c$ denotes the tensile strain of cohesive bridges, which can be related with the fabric strain by

$$\hat{\epsilon}^c = \hat{\epsilon}_r^c - \hat{\epsilon}_v^e. \tag{17}$$

Therein $\hat{\epsilon}_r^c$ is a reference value which exceeds $\hat{\epsilon}^c$ due to $\hat{\epsilon}_v^e > 0$ (compression of fabric and tensile strain of bridges positive). $\hat{\epsilon}_c^c$ in (16) denotes $\hat{\epsilon}^c$ at a critical point of cohesive bridges, and $\hat{\epsilon}_0^c$ denotes $\hat{\epsilon}^c$ for $\hat{w}_c = 0$. Thus the effective stress, which transfers momentum in the solid rock mass, is

$$\hat{\sigma}'_{ij} = (1 - \hat{\mu})\frac{\partial \hat{w}}{\partial \hat{\epsilon}_{ij}^e} = (1 - \hat{\mu})[\frac{\partial \hat{w^e}}{\partial \hat{\epsilon}_{ij}^e} + \frac{\partial \hat{w^c}}{\partial \hat{\epsilon}^c}] = \hat{\sigma}_{ij}^f - \delta_{ij}\hat{p}^c \tag{18}$$

with a reduction factor $1 - \hat{\mu}$ depending on the eutaraxy $\hat{\chi}$ as for sand (A3). $\hat{\sigma}_{ij}^f$ denotes the fabric stress including the additional pressure $\hat{p}^c$, which with (16), (17) and (18) is

$$\hat{p}^c = (1 - \hat{\mu})\frac{\partial \hat{w}_c}{\partial \hat{\epsilon}^c} = (1 - \hat{\mu})\hat{C}\hat{s}_c(1 - \frac{\hat{\epsilon}^c - \hat{\epsilon}_c^c}{\hat{\epsilon}_0^c - \hat{\epsilon}_c^c}). \tag{19}$$

Therein $\hat{s}_c$ denotes the area of cohesive bridges per volume of the sample, and $\hat{C}$ their specific surface energy.

The evolution of the friction factor $\hat{b}$ could be approximated by means of (5). An evolution equation for $\hat{s}_c$ could be added with $\hat{s}_c \to 0$ for continued dilation. The reference values $\hat{\epsilon}_r^c$ and $\hat{\epsilon}_0^c$ do not matter for critical phenomena, they could be calibrated as indicated under Fig. 4. A subsequent contractant collapse could also be captured by means of (14) and (18), but the validation gets more difficult due to autogeneous changes of p_w. The multi-fractality could be captured by a relation of $\hat{\mu}$ and the variable fractal exponent α as for sand (A3).

Like with sand these constitutive relations can be written with tensors and invariants beyond axial symmetry. With (18) the symmetry $\hat{\epsilon}_{ij}^e = \hat{\epsilon}_{ji}^e$ implies $\hat{\sigma}'_{ij} = \hat{\sigma}'_{ji}$, and stress-aligned orthogonal anisotropy of the differential stiffness matrix $M_{ijkl} \equiv \partial \hat{\sigma}'_{ij} / \hat{\epsilon}_{kl}^e$. Beyond the elastic range the evolution of elastic strain can be captured by

$$\hat{\dot{\epsilon}}_{ij}^e \equiv \hat{D}_{ij}^e = (1 - \hat{\mu}) \hat{D}_{ij} - \hat{\chi} (\hat{D}_{ij}^e - h \hat{D}_v^e) \hat{D}. \tag{20}$$

Therein $\hat{D}_{ij}$ denotes the quasi-local stretching rate tensor (A2), $\hat{D}$ its amount and $\hat{D}_{ij}^e$ its elastic part. Its symmetry $\hat{D}_{ij} = \hat{D}_{ji}$ by definition implies the symmetry $\hat{\epsilon}_{ij}^e = \hat{\epsilon}_{ji}^e$ by (20), which means also $\hat{\sigma}'_{ij} = \hat{\sigma}'_{ji}$ by (18). The auxiliary parameter h, the evolution of the eutaraxy $\hat{\chi}$ and its relation with the reduction parameter $\hat{\mu}$ and the fractal exponent α can be approximated as for sand (A3). The evolution of the internal pressure $\hat{p}_c$ can also be generalized from the one with axial symmetry. Like with sand (Gudehus 2019) this leads to dilatancy alongside with a growth of the invariant ratio $\hat{\tau}/\hat{p}'$, and to contractancy with a reduction of $\hat{\tau}/\hat{p}'$.

References

Alejandro L. and Alonso E. (2005): Considerations of the dilatancy angle in rocks and rock masses. *Intern. Journ. Rock Mech. Ming. Sci.*, 42/4, 481-507.

Althaus E., Fritz-Töpfer A., Lempp C. and Natau O. (1994): Effects of Water on Strength and Failure Mode of Coarse-Grained Granite at 300^o C. *Rock Mech. Rock Engg.*, 27/1, 1-21.

Bak P., Tang C. and Wiesenfeld K. (1987): Self-organized criticality: An explanation of 1/f noise. *Phys. Rev. Lett.*, 59/4, 381-384.

Balthasar K., Gudehus G., Külzer M. and Libreros-Bertini A.-B. (2006): Thin layer shearing of a highly plastic clay. *Nonlin. Processes in Geophys.*, 13, 671-680.

Brady B.T. and Rowell B.A. (1986): Laboratory investigation of the electrodynamics of rock fracture. *Nature*, 3, 21-29.

Burridge R. and Knopoff L. (1967): Model and theoretical seismicity. *Bull. Seis. Soc. Amer.*, 57, 341-371.

Cauchy A.-L. (1827): De la pression ou tension dans un corps solide. *Exercices de Mathémathique*, 2, 389-440.

Cieslik J. (2018): Dilatancy as a measure of fracturing development in the process of rock damage. *Open Geoscience*, 10/1, 484-490.

Coulomb C.A. (1776): Essai sur une application des regles de maximis et minimis a quelques problemes de statique relatifs a l'architecture. *Mémoires de mathématique et de physique, par divers savants*, Vol. 7.

Dahmen K.A. and Ben-Zion Y. (2009): Jerky Motion in Slowly Driven Magnetic and Earthquake Fault Systems. In: Meyers, R. (ed.): *Encyclopedia of Complexity and System Science*, 5021-5037, Springer.

Darwin G. (1883): On the horizontal thrust of a mass of sand. *Proc. Inst. Civ. Eng.*, Vol. LXXL, 350-378, London.

Desrues J., Besuelle P. and Lewis H. (2007): Strain Localization in Geomaterials. *Geol. Soc, London*, Spec. Publ., 289, 47-73. DOI: 10.1144/SP289.4

Frischbutter A., Neon D., Scheffzük C., Vrana M. and Walther K. (2000): Lattice strain measurements on sandstones under load using neutron diffraction. *Journ. Struct. Geol.*, 22, 1587-1600.

Griffith A .A. (1922): The Phenomena of Rupture and Flow in Solids. *Philos. Trans. Roy. Soc. London*, A: Mathematical, Physical and Engineering Sciences., 221, 582-593.

Gudehus G. (2011): Physical Soil Mechanics. 840 p., Springer.

Gudehus G. (2019): Granular solid dynamics with eutaraxy and hysteresis. *Acta Geotechn.*,15, 1173-1187. https://doi.org/10.1007/s11440-019-00820-y

Gudehus G. (2020): Implications of the principle of effective stress. *Acta Geotechnica*, 16,1939-1947. DOI:10.1007/s11440-020-01068-7

Gudehus G.and Lempp, C. (2022): Tectonic Critical Phenomena with Dilatancy in Lithosphere Sections. *Hall. Jb. Geowissenschaften*, 45, 33-58.

Gudehus G and Touplikiotis A. (2016): Wave propagation with energy diffusion in a fractal solid and its fractional image. *Soil Dyn. Earthquake Engng.*, 89, 38-48.

Hardenberg W. (2011) Expecting Disaster: The 1963 Landslide of the Vajont. *Arcadia, 8 - Arcadia Collection: Technology and Expertise.*
https://www.environmentandsociety.org/arcadia/expecting-disaster-1963-landslide-vajont-dam

Holland M., Urai J.L. and Martel S. (2006): The internal structure of fault zones in basaltic sequences. *Earth Plan. Sci. Lett.*, 248, 301–315.

Hubbert M. K. (1937): Theory of scale models as applied to the study of geologic structures. *Geological Society of America Bulletin*, 48/10, 1459–1520.

Jiang Y. and Liu M. (2009): Granular solid hydrodynamics. *Granular Matter*, 11, 139-145.

Kadanoff L.P. (1966): Scaling laws for Ising models near T_c. In: *Physics Physique Fizika*, 2/6, 263-272.

Kadanoff L.P. (1999): Built upon sand: Theoretical ideas inspired by the flow of granular materials. *Rev. Mod. Phys.*, 71/1, 435-444.

Kolymbas D. (1981): Bifurcation Analysis for Sand Samples with a Non-Linear Constitutive Equation. *Ingenieur-Archiv*, 50, 131-140.

Kolymbas D. (2003): Fractals in Geomechanics. Intruduction to a workshop, *Publ. Inst. Geotechnics*, University Innsbruck.

Leary P.C. (1997): Rock as a critical-point system and the inherent implausibility of reliable earthquake prediction. *Geoph. J. Int.*, 131, 451-466. https://doi.org/10.1111/j.1365-246X.1997.tb06589.x

Lempp C. and Natsu O. (1985): Mechanische Eigenschaften von Störungen und Verwitterungszonen im Granitgebirge und deren genetische Charakterisierung. *In: Heitfeld, K.-H. (ed.): Ingenieurgeologische Probleme im Grenzbereich zwischen Locker- und Festgestein*, 695 p., Springer.

Lempp C. (1994): Experimentelle Untersuchungen zur geomechanischen Wirkung von Gesteinsfluiden. *Veröff. Inst. Boden- und Felsmechanik*, 135, 202 p., Univ. Karlsruhe.

Lempp C., Shams K.M. and Jahr N. (2012): Approaches to stress monitoring in deep boreholes for future CCS projects. *Environ. Earth Sci*, 67, 435–445.

Lempp C., Menezes F. and Schöner A. (2020): Multi-stage triaxial tests with water-saturated sandstones - a microtectonic study with a fractal perspective. *Journal of Structural Geology*, https://doi.org/10.1016/j.jsg.2020.104092.

Li L., Hu J., Li S., Qin C., Liu H., Chen D. and Wang J (2021): Development of a Novel Triaxial Rock Testing Method Based on Biaxial Test Apparatus and Its Application. *Rock Mech. Rock Engng.*, online edition.

Luong M.P. (1982): Mechanical aspects and thermal effects of cohesionless soils under cyclic and transient loading. *Proc. IUTAM Conf. Deform. Failure Gran. Mat.*, Delft, 239-264.

Mandelbrot B. (1982): *The fractal Geometry of Nature.* 460 p., Freeman, New York.

Mandelbrot B. (1999): *Multifractals and 1/f-noise - wild self-affinity in physics.* 450 p., Springer.

Mandl G. (1988): *Mechanics of Tectonic Faulting, Models and Basic Concepts.* 407 p., Elsevier.

Menezes F. (2022): Stress-dilatancy relations for water-saturated sandstone samples. Under preparation for *Acta Geot.*

Morgenstern N.R. and Tchalenko J.S. (1967): Microspopic structures in kaolin subjected to direct shear. *Géotechnique*, 17, 309-328.

Nübel K. (2002): Experimental and numerical investigation of shear localization in granular material. *Dissertation Univ. Karlsruhe. Veröff. Inst. für Boden- und Felsmechanik der Univ. Karlsruhe.*, 159.

Ord A. and Hobbs B.E. (2010): Fracture pattern formation in frictional, cohesive, granular material. *Phil. Trans. R. Soc. A, 368, 95–118.*

Peletier L.A. and Troy W.C. *(2001): Spatial Patterns: Higher Order Models in Physics and Mechanics.* Progress in Nonlinear Differential Equations and Their Applications*, 45, 343 p., Birkhäuser.*

Persson B.N.J. *(2000a): Theory of time-dependent plastic deformation in disordered solids.* Phys. Rev. B*, 61/9, 5949-5966.*

Persson B.N.J. *(2000b):* Sliding Friction - Physical Principles and Applications*. 516 p., Springer.*

Reynolds O. *(1885): On the dilatancy of media composed of rigid particles in contact, with experimental illustrations.* Philosophical Magazine*, 20, 469-481.*

Roscoe K.H. *(1970): The influence of strains in soil mechanics.* Géotechnique*, 20/2, 129-170.*

Rosenau M., Corbi F. and Dominguez S. *(2016): Analogue earthquakes and seismic cycles: Experimental modelling across timescales.* Solid Earth *Discussions.*

Rowe P.W. *(1962): The stress-dilatancy relation for static equilibrium of an assembly of particles in contact.* Proc. Roy. Soc. London*, A 269, 500-527.*

Sornette D. *(2000):* Critical Phenomena in Natural Sciences*. 434 p., Springer.*

Tarasov V.E. *(2005): Continuous Medium Model for Fractal Media.* Physics Letters*, A 336, 167-174.*

Taylor D.W. *(1948):* Fundamentals of soil mechanics*. 700 p., J. Wiley and Sons.*

Terzaghi K. *(1936): The shearing resistance of saturated soils and the angle between the planes of shear.* Proc.1st Int. Conf. on Soil Mechanics, *Contr. D7, Harvard.*

Truesdell C. and Noll W. *(2004):* The Non-Linear Field Theories of Mechanics. *602 p., Springer.*

Turcotte D.L. *(2001): Self-organized criticality: Does it have anything to do with criticality and is it useful?* Nonlinear Processes in Geophysics, *8, 193-196.*

Vardoulakis I. and Sulem J. *(1995):* Bifurcation analysis in geomechanics. *462 p.,Taylor and Francis eBooks.*

Vardoulakis I. *(1996): Deformation of water saturated sand: I. Uniform undrained deformation and shear banding; II. The effect of pore-water flow and shear banding.* Géotechnique, *46, 441–472.*

Vrolijk P.J., Urai J. and Kettermann M. *(2016): Clay smear: Review of mechanisms and applications.* Journal of Structural Geology, *86, 95-152.*